Influence of Hydrogen Content on Axial Fracture Toughness Parameters of Zr-2.5Nb Pressure Tube Alloy in the Temperature Range of 306-573 K

Singh, Ram Nivas; Ståhle, Per; Iyengar, Srinivasan

Published in:
Proceedings of ICAPP'06, Reno NV USA, June 4-8,2006, paper 6138

2006

Proceedings of ICAPP '06
Reno, NV USA, June 4-8, 2006
Paper 6138

Influence of Hydrogen Content on Axial Fracture Toughness Parameters of Zr-2.5Nb Pressure Tube Alloy in the Temperature Range of 306-573 K

R. N. Singh[1], P. Ståhle[1,2] and N. S. Srinivasan[2]
[1] Materials Science, Technology and Society, Malmö University, SE20506, Sweden
[2] Department of Mechanical Engineering, Lund Institute of Technology, Lund University, Box 118, SE22100 LUND, Sweden
Email: Ram.Singh@ts.mah.se Tel. +46-40-6657704 FAX: +46-40-6657135

Abstract- *Hydrides are suspected to be fracture initiating sites in Zr-alloys and the presence of hydride platelets normal to tensile load significantly influences crack propagation. However, the role of hydrides in crack nucleation and its propagation and influence of temperature on the same has not been delineated clearly. In this work, influence of hydrogen and temperature on the axial fracture toughness parameters of Zr-2.5Nb pressure tube alloys is reported. The fracture toughness tests were carried out using 17 mm width curved compact tension specimens machined from gaseously hydrogen charged tube-sections and tested in the temperature range of 306 to 573 K. Metallography of the samples revealed that hydrides were predominantly oriented along axial-circumferential plane of the tube. The fracture toughness parameters like J_Q, $J_{0.15}$, J_{Max}, $J_{1.5}$, dJ/da, K_{JC} and K_{Max} were determined as per the ASTM standard E-813, with the crack length measured using direct current potential drop technique. The plane strain K values were computed from the corresponding J values. The critical crack length for catastrophic failure was determined using a numerical method, which is widely used in literature. It is observed that for a given test temperature both the fracture toughness parameters representing crack initiation, such as J_Q, $J_{0.15}$ and K_{JC} and crack propagation, such as J_{Max}, $J_{1.5}$, and K_{Max}, decrease mildly with increase in hydrogen content whereas mean dJ/da is practically unaffected by hydrogen content. Also, for a given hydrogen content crack initiation fracture toughness parameters showed large scatter with a tendency to decrease with increase in test temperature whereas the crack propagation fracture toughness parameters increased with temperature to a saturation value.*

I. INTRODUCTION

About ninety water-cooled nuclear reactors in the world, which are either in operation or are under construction, use pressure tubes instead of pressure vessels to contain the hot pressurized coolant. These reactors are cooled and moderated by heavy water and hence are known as Pressurized Heavy Water Reactor (PHWR)[1]. Each coolant channel assembly of PHWRs comprises of a pressure tube, a calandria tube and garter springs. Natural uranium oxide powder compacted and sintered in the form of pellets and encapsulated in thin cladding, forms the fuel pins of the PHWRs. Several such pins are assembled in the form of fuel bundles and are loaded in horizontal pressure tubes. Pressure tubes (PT) act as miniature pressure vessel in PHWRs with coolant heavy water flowing through it under a pressure of around 10 MPa and at a temperature in the range of 523 to 573 K. Calandria tubes (CT) surrounds the pressure tubes from outside. Garter springs are provided at regular interval in the annular space to support pressure tube and prevent it from contacting the calandria tube, which is surrounded by low pressure, low temperature heavy water moderator maintained at 333 K in a large stainless steel vessel called calandria vessel.

The use of natural UO_2 as fuel in PHWRs demands that the core structural materials such as cladding tubes (also called fuel tubes), pressure tubes (coolant tubes), calandria tubes and garter springs must have low neutron absorption cross-section and should satisfy the physical, mechanical, metallurgical and chemical requirements in radiation environment[2-4]. Pressure tubes being the final pressure boundary containment structures in PHWRs, their integrity is to be maintained during reactor operation[5-7]. Though the specification limit for hydrogen content in the pressure tubes is 5 ppm for quadruple melted and 25 ppm by weight for double melted Zr-2.5Nb pressure tubes[8-9], part of the hydrogen/deuterium evolved during service from coolant-metal corrosion reaction is picked up by the pressure tubes[10-11]. Hydrogen present in excess of terminal solid solubility (TSS)[12-13] precipitates out as hydride phase. Being brittle, the presence of

substantial quantities of hydrides can cause embrittlement of the host matrix resulting in loss of ductility, impact and fracture toughness. However, for a significant reduction in these properties, certain minimum volume fraction of the embrittling phase[11] is required and degree of embrittlement is strongly influenced by the orientation of hydride platelets.

Since hydride embrittlement is a major life limiting factor for the components made from these alloys, several theoretical and experimental studies have been carried out to understand the influence of hydrogen/hydride on the mechanical properties in general and micromechanisms assisting crack nucleation and its propagation in the presence of hydride, in particular[9,14-20]. For ductile materials like Zr-alloys, crack initiation follows void nucleation and its growth in the plastic zone[21]. Nucleation of voids is associated with fracture of second phase particle or separation of matrix-precipitate interface. Hydrides are suspected to be fracture initiating sites in Zr-alloys and the presence of hydride platelets normal to tensile load significantly influences crack propagation. However, the role of hydrides in crack nucleation and its propagation and influence of temperature on the same has not been delineated clearly.

The texture of the CWSR Zr-2.5Nb alloy is such that crystallographically, only two hydride platelet orientations are permissible, viz., along the circumferential-axial and the radial-axial planes[11,22], which are respectively called circumferential and radial hydrides, as illustrated schematically in figure 1. The microstructure of the CWSR Zr-2.5Nb alloy pressure tube material is such that under unstressed condition, only circumferential hydrides form[11]. However, during power shut down, when pressure tubes are cooled under hoop stress dissolved hydrogen may precipitate as radial hydrides, which being oriented normal to hoop stress direction are extremely detrimental to the integrity of the pressure tubes[11,]. The presence of radial hydride is reported to make Zr-2.5 Nb alloy containing 50 wppm of hydride significantly brittle below 423 K with reduction in area reported to be zero at ambient temperatures[11,22].

The objective of the present investigation is to estimate the influence of hydrides on the fracture initiation and fracture propagation toughness of Zr-2.5 Nb pressure tube alloy in the temperature range of ambient (306 K) to the reactor operating temperature of 573 K. It is felt that the presence of radial hydrides makes this alloy so brittle[22] that distinction between fracture initiation and propagation toughness will not be meaningful and hence for this investigation Zr-2.5Nb pressure tube material was hydrided under zero externally applied stress to ensure the selective precipitation of circumferential hydrides only. The fracture toughness parameters like J_Q, $J_{0.15}$, J_{Max}, $J_{1.5}$ and *dJ/da* were determined as per the ASTM standard E-813, with the crack length measured using direct current potential drop technique. The plane strain K values such as K_{JC} and K_{JMax} were computed from the corresponding J values. The critical crack length for catastrophic failure was determined using a numerical method, which is widely used in literature[23].

II. EXPERIMENTAL

II.A Material and Specimen

The material used in this study for fracture toughness tests were from double melted, autoclaved, unirradiated Zr-2.5Nb pressure tube (spool number 100-2-3) of PHWR 235 Mwe. The internal diameter of the tube was 81.5 mm with wall thickness of 3.7 mm. The chemical analysis indicated Nb and O contents to be 2.54 and 0.1175 wt % respectively. The room temperature yield and ultimate tensile strength of the material was 599 and 833 Mpa respectively and the tensile elongation was 13.3 % in 25 mm gage length. The pressure tube sections of length 110 mm were polished up to 1200 grit emery paper to obtain oxide free surface and subsequently these tube sections were gaseously charged with target hydrogen concentration of 20 or 60 or 100 ppm by weight in a modified Sivert's type apparatus. Curved Compact Toughness (CCT) specimens of width 17 mm were machined from these spools. The crack plane was along axial-radial plane to facilitate crack propagation along axial direction of the tube. The hydrogen content estimated by inert gas fusion technique using a LECO analyzer were 21, 70 and 90 ppm corresponding to the target concentration of 20, 60 and 100 ppm.

II.B Fracture Toughness Testing

The fracture toughness testing procedure recommended in ASTM standard E-813 was followed in the present investigation except for the fact that the crack length was determined using direct current potential drop (DCPD) technique[14,15], which facilitated the use of Single specimen technique for fracture toughness parameter determination. A sharp crack tip was obtained by fatigue precracking the CCT specimens using a MTS make servo-hydraulic universal testing machine. Due to curvature of the CCT specimens tapered pins were used to obtain uniform crack front across the thickness of the specimen. The stress intensity factor, K_I, for fatigue precracking, calculated using *equation 1*, was reduced in six steps from the starting value of 20 to the final value of 8 Mpa.m$^{1/2}$ with the ratio of minimum to maximum load being maintained around 0.1.

$$K_I = \frac{P_Q}{BW^{1/2}} f(a/W) \qquad (1)$$

where

$$f\left(\frac{a}{W}\right)=\frac{\left[2+\frac{a}{W}\right]\left[0.886+4.64\frac{a}{W}-13.32\left(\frac{a}{W}\right)^2+14.72\left(\frac{a}{W}\right)^3-5.6\left(\frac{a}{W}\right)^4\right]}{\left(1-\frac{a}{W}\right)^{3/2}}$$

[24].

The value of a/W after fatigue precracking was about 0.5. An Instron make screw driven UTM was used to pull the fatigue precracked specimen in tension to facilitate mode I crack propagation on the axial-radial plane along axial direction of the tube. A resistance heated three-zone furnace fitted on the UTM was used for attaining high temperature. The specimen was heated in air to the test temperature, soaked for an hour before starting the test. The specimens were pulled at a cross-head speed of 0.5 mm/min. The temperature of the testing furnace was controlled during the test within 1K through a K-type thermocouple, placed very close to the heating element, using a programmable temperature controller. The temperature of the CCT specimens was monitored using K-type thermocouple (0.2 mm dia.) spot welded to the inside curvature of the CCT specimens within 1 mm of the fatigue precrack tip. Two additional thermocouples were placed on the lower and upper grip touching the specimen. The crack growth was monitored using direct current potential drop technique[14-15]. A constant DC current of 6 Amperes was used for all specimens. The DCPD output was measured using 0.5 mm diameter Zr-2.5Nb wires spot-welded to the crack opening within 1 mm of the each side of the notch. The DCPD and thermocouple outputs were continuously recorded on a 12-channel video graphic recorder. Apart from estimating the fatigue precrack length from DCPD data, the fatigue precrack length was also computed from the nine equispaced readings from the fractograph obtained from the broken half of the specimens after fracture tests. The average of the first and ninth reading was added to the sum of the remaining seven readings and the resulting sum was divided by eight to obtain the fatigue crack length.

II.C Computations

The crack length was computed from the DCPD values as described in our earlier work[24]. The area, A_{pl}, was obtained from load vs. load line displacement curve for a given crack length and represents the energy required for causing plastic deformation. The *J* values were split into elastic and plastic part (ASTM E 813) as per *equation 2*:

$$J=J_{el}+J_{pl}=\frac{K^2(1-\nu^2)}{E}+\frac{\beta A_{pl}}{Bb} \quad (2)$$

where $\beta=2\frac{(1+\alpha)}{(1+\alpha^2)}$ with

$\alpha=\left[(2a_0/b)^2+2(2a_0/b)+2\right]^{1/2}-\left[(2a_o/b)+1\right]$.

The Blunting line computed using $J_{blunt}=2\sigma_{flow}(\Delta a)$, where $\sigma_{flow}=(\sigma_{YS}+\sigma_{UTS})/2$, was superimposed over *J* vs *Δa* plot. Two exclusion lines parallel to the blunting line were drawn at an offset of 0.15 and 1.5 mm crack length extension. The data falling in between the exclusion lines were fit to a power law ($J=C_1\Delta a^{C_2}$) and straight line. Another offset line parallel to the blunting line was drawn at an offset of 0.2 mm and the intersection point of the 0.2 mm offset line with the power law curve passing through the qualified data was taken as the J_Q value. The slope of the best fit line yielded the mean *dJ/da* value. For each test the *J* values corresponding to a crack length of 0.15 and 1.5 mm and maximum load were also noted. Since Zr-2.5Nb pressure tube alloy is ductile a valid K_{IC} test cannot be performed on the pressure tube material of 3.7 mm thickness. Hence, the values of K_{JC} and K_{JMax} were computed corresponding to J_Q and J_{Max} under plane strain condition as per *equation 3*.

$$K_J=\sqrt{\frac{J\,E}{1-\nu^2}} \quad (3)$$

where Young's modulus $E=95900-57.4(T-273)Mpa$ [25] and $\nu=0.436-4.8X10^{-4}(T-300)$ [25] were used. The critical crack length (*CCL*) values for the catastrophic failure of the pressure tube under the PHWR operating condition were computed from corresponding J_Q values by iterative method as per *equation 4* [23].

$$J_Q=\frac{8a\sigma^2_{flow}}{\pi E}\ln[\sec(\pi MS_H/2\sigma_{flow})] \quad (4)$$

where $a=1/2\,CCL$ and $\sigma_{flow}=907-0.7544T$ Mpa, and hoop stress, $S_H=\frac{PD}{2B}$.

The aforementioned fracture toughness parameters were determined as a function of hydrogen content in the temperature range of 306 to 573 K. For metallography, the specimens were sectioned along radial-circumferential and radial-axial plane of the pressure tube. Standard metallographic technique was followed to reveal the hydride microstructure, its morphology and distribution. For optical microscopy the specimens were etched in a solution of $HF:HNO_3:H_2O$::2:9:9 for 15 seconds. Fracture surfaces were examined under scanning electron microscope in backscattered mode.

III. RESULTS

III.A Microstructure

The current fabrication route of CWSR Zr-2.5 wt. % Nb pressure tubes produces a two phase microstructure of strongly textured and elongated (in axial direction) α-grains surrounded by very thin nearly continuous β-phase network along the grain-boundaries[26]. The α-grains, possess HCP structure, with basal poles predominantly aligned in the

circumferential (transverse) or radial direction of the tubes. Figure 1 shows the three orthogonal directions of the pressure tube viz. Axial (A), Circumferential (C) and Radial © and AR – Axial-Radial, RC – Radial-Circumferential and AC – Axial-Circumferential planes schematically. Crystallographically permitted orientation of the hydride platelets in Zr-2.5Nb pressure tube alloy is also shown in this figure[11]. Typical α grain dimensions for the cold worked and stress-relieved Zr-2.5Nb pressure tube material is also indicated in this figure[26].

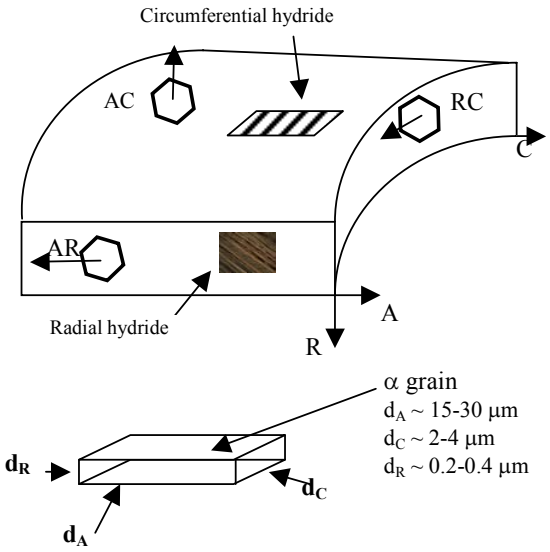

Fig. 1 A tube section illustrating the orientation of circumferential and radial hydrides[11] along with α phase grain dimensions[26] observed in CWSR Zr-2.5Nb pressure tube alloy.

The microstructural features of hydrides on two orthogonal planes (AR and RC) of the Zr-2.5Nb pressure tube material, charged with about 100 wt. ppm of hydrogen, are shown in fig. 2. This figure shows that in the as-hydrided condition, the traces of the hydride platelets (dark lines) are oriented along the circumferential direction only. These hydrides are called circumferential hydrides. This selective formation of circumferential hydrides (oriented along the axial-circumferential plane of the pressure tube) in the as-hydrided condition is attributed to the microstructure of the pressure tubes[11]. It may be noted from fig. 2(a & b) that the trace on radial-axial plane is straight (with minimum irregularity or serrations) and longer than that on radial-circumferential plane. This is expected because the longer α phase grain dimension along axial direction of the pressure tube[26] provides uninterrupted growth along axial direction. The branching of the trace of the hydride on the radial-circumferential plane is due to shorter grain dimension along the circumferential direction[26] of the pressure tube (Fig 1). Since habit plane[27] of hydrides in α phase is nearly parallel to the basal plane, for the texture of the pressure tube[11,26] one out of every three α phase grains will have favorable texture. Thus, hydrides cannot grow straight along the circumferential direction. Instead, within every 2-4 μm they will branch out to grow along the favorably oriented grains. This could be the reason for longer and straighter hydride trace along axial direction compared to shorter and branched hydride trace along the circumferential direction of the pressure tube material.

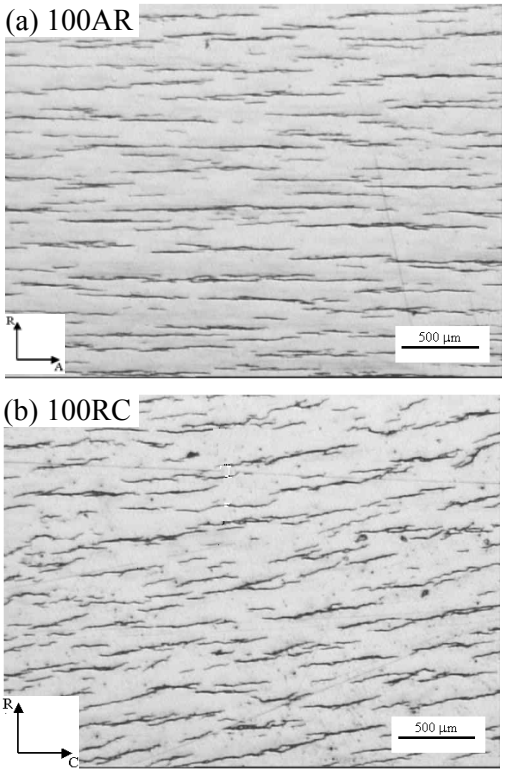

Fig. 2 The microstructure of Zr-2.5Nb pressure tube alloy charged with 100 wt. ppm of hydrogen revealing traces of hydrides (dark lines) on two orthogonal planes (AR and RC) defined in fig. 1. Arrow shows the direction.

The fractographic features shown in Fig. 3 correspond to the samples which were tested at ambient temperature i.e. 306 K and were containing (a) 21 and (b) 70 ppm of hydrogen. The fatigue precracked region on the left side of the fractographs can be seen to contain traces of hydride (dark lines). The fracture region exhibits large number of penny shaped mesocracks oriented normal to the crack propagation plane. These mesocracks like hydride platelets were also oriented along the CA plane of the tube and hence will be designated as CA-mesocracks henceforth in this manuscript. Also, CA-mesocracks were not seen near the edge of the sample thickness. The fractographs in fig. 3(a&b) suggest that with increasing hydrogen content, the length of the CA-mesocracks increase, which probably could be due to hydrides facilitating the interlinking of the mesocracks.

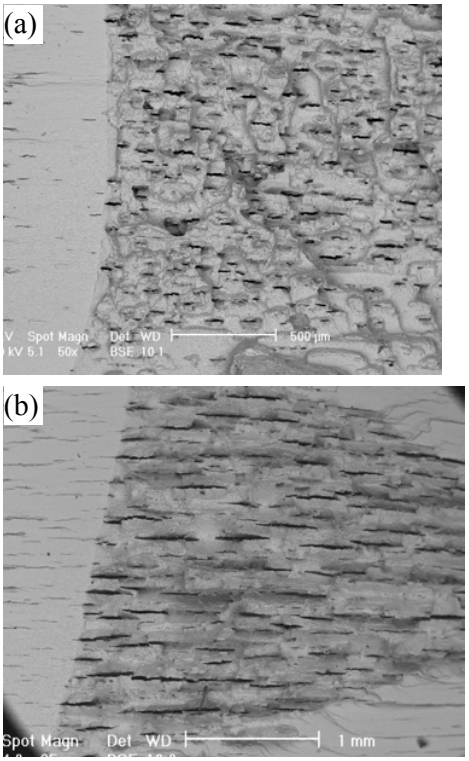

Fig. 3 Fracture surface of the samples tested at 306 K and containing (a) 21 ppm and (b) 70 ppm of hydrogen as seen under Scanning electron microscope under backscattered mode.

III.B Influence of Hydrogen Content

Fig. 4 depicts a typical J vs Δa curve for the sample containing 70 ppm of hydrogen and tested at 306 K. The blunting and exclusion lines are also shown in this fig. to illustrate the computation of J_Q. The intersection of the 0.2 mm offset line and the best fit power law curve passing through the qualified J values were taken as J_Q. Apart from J_Q, the J values corresponding to the Δa of 0.15 mm, 1.5 mm and maximum load were also recorded. The slope of the best fit line passing through the qualified J values were taken as the mean dJ/da.

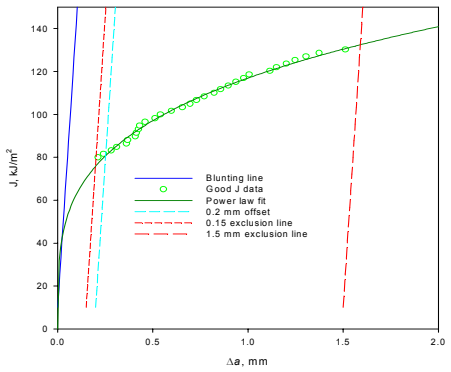

Fig. 4 A typical J vs Δa curve for the sample containing 70 ppm of hydrogen and tested at 306 K along with blunting and exclusion lines illustrates J_Q computation.

Fig. 5 shows the influence of hydrogen content on (a) J_Q and J_{Max}, (b) $J_{0.15}$ and $J_{1.5}$, (c) mean dJ/da and (d) K_{JC} and K_{JMax} values for Zr-2.5Nb pressure tube alloys at various temperatures. The fracture toughness parameters such as J_Q, $J_{0.15}$ and K_{JC} represent the fracture initiation toughness. The dependence of these parameters on hydrogen content shows negative slope at all the test temperatures suggesting that the values of the aforementioned fracture initiation parameters decreases with increase in hydrogen content. However, the dependence of these parameters on hydrogen content is very weak with magnitude of slopes being less than 0.15, except for the test temperature of 523 K for which the magnitude of slope is greater than 0.32. The fracture toughness parameters such as J_{Max}, $J_{1.5}$, dJ/da and K_{JMax} can be thought to represent the resistance to crack propagation and influence of hydrogen content on these parameter can also be seen in fig.5. The $J_{1.5}$ values shows negative slope at all test temperatures suggesting the enhancement of embrittling effect of hydrogen (fig. 5(b), which was observed to be more pronounced in the temperature range of 373-573 K compared to that at 306 K. The influence of hydrogen content on J_{Max} values and corresponding K_{JMax} values are not in good agreement. While at 306 and 573 K both J_{Max} values and corresponding K_{JMax} values increased with increasing hydrogen content at intermediate test temperatures of 373 and 523 K their values decreased with increase in hydrogen content. This trend is summarized by the very weak dependence of mean dJ/da on hydrogen content with the magnitude of slope being less than 0.14.

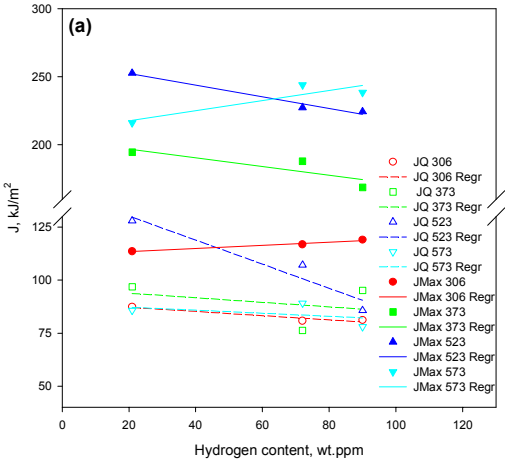

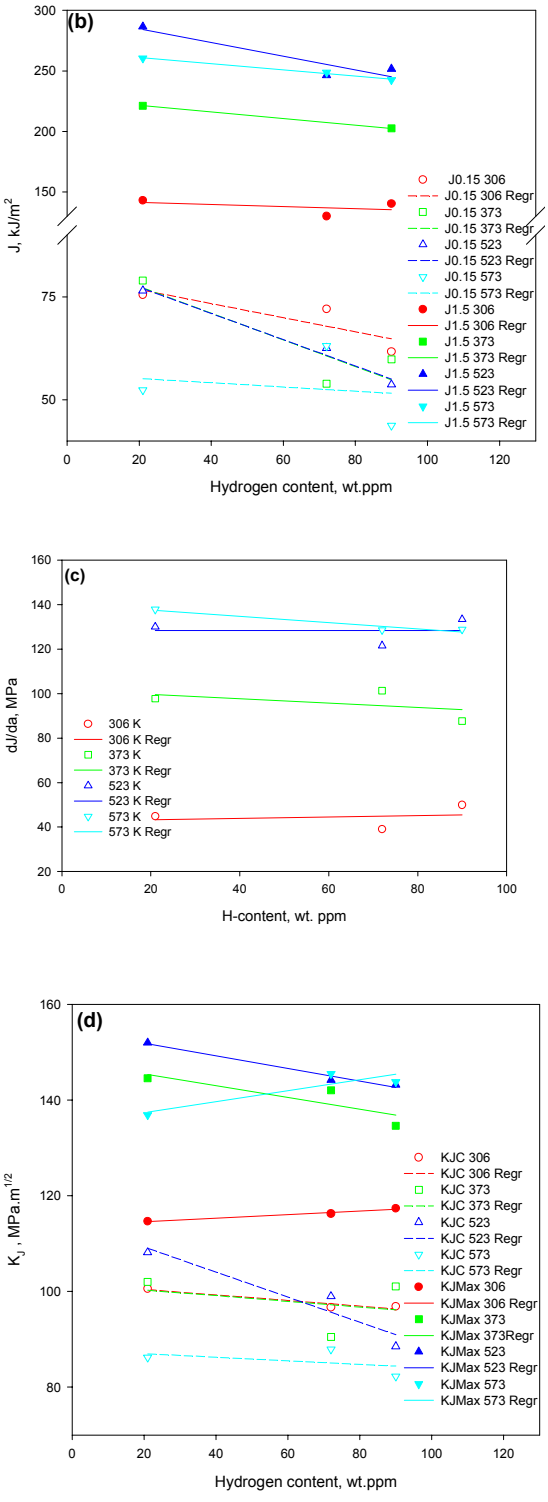

Fig. 5 Influence of hydrogen content on (a) J_Q and J_{Max}, (b) $J_{0.15}$ and $J_{1.5}$, (c) dJ/da and (d) K_{JC} and K_{JMax} values of Zr-2.5Nb pressure tube alloy at various test temperatures.

III.C Influence of Test Temperature

The Influence of test temperature on (a) J_Q and J_{Max}, (b) $J_{0.15}$ and $J_{1.5}$, (c) mean dJ/da and (d) K_{JC} and K_{JMax} values of Zr-2.5Nb pressure tube alloy containing different amount of hydrogen is shown in Fig. 6. The fracture initiation parameters such as J_Q, $J_{0.15}$ and K_{JC} appear to be mildly decreasing with increase in test temperature, though for the samples containing 21 wt. ppm of hydrogen the scatter in data was large. The crack propagation parameters such as J_{Max}, $J_{1.5}$, mean dJ/da and K_{JMax} increased with increase in test temperature and appear to be reaching a saturation value at higher test temperatures suggesting that these data represent the high temperature part or upper shelf of the typical S-curve exhibited by the temperature dependence of fracture energy. It may be noted that the mean dJ/da data showed least scatter compared to other parameters. Also, the difference between crack initiation fracture toughness parameters and crack propagation parameters increases with increase in test temperature.

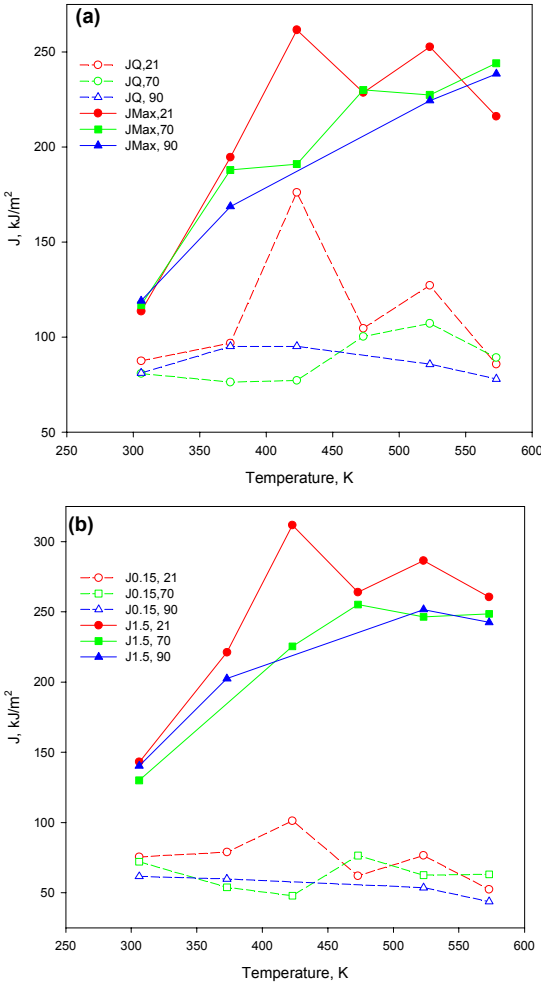

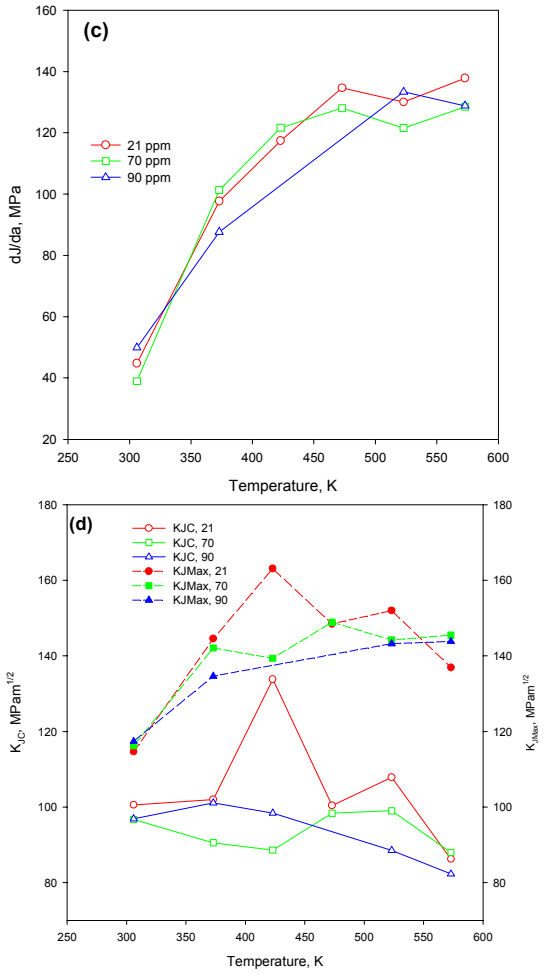

Fig.6 Influence of test temperature on (a) J_Q and J_{Max}, (b) $J_{0.15}$ and $J_{1.5}$, (c) dJ/da and (d) K_{JC} and K_{JMax} values of Zr-2.5Nb pressure tube alloy containing different amount of hydrogen.

III.D Critical Crack Length

The variation in critical crack length for the catastrophic failure of pressure tubes under reactor operating condition with hydrogen content and test temperature is listed in Table 1. The value of *CCL* determined in the present investigation was > 54 mm for all the hydrogen concentrations and test temperatures. Except at 423 K the influence of hydrogen content on *CCL* was not very significant. The *CCL* values were observed to increase with increase in test temperature for the samples containing 21 ppm hydrogen in the temperature range of 306 to 423 K, and thereafter it was observed to be decreasing with further increase in test temperature. For the samples containing higher amount of hydrogen, the influence of test temperature on *CCL* was not significant.

Table 1: CCL (mm) for catastrophic failure of Zr-2.5Nb pressure tubes under PHWR operating condition computed from J_Q values obtained in this work at various test temperatures and hydrogen contents.

S. No.	Temperature, K	21 wt. ppm	70 wt. ppm	90 wt. ppm
1.	306	57.6	56.0	56.0
2.	373	59.6	54.8	59.2
3.	423	73.0	55.0	59.2
4.	473	61.2	60.4	--
5.	523	65.6	61.8	57.2
6.	573	57.2	58.0	55.2

IV. DISCUSSION

The variation in the critical specimen dimension such as specimen thickness, B, and uncracked ligament, b_o, for a valid J_{IC} yielding material specific fracture toughness with test temperature is shown in fig. 7. The specimen thickness and the uncracked ligament length used in the present investigation are also superimposed in this fig. It is evident from this fig. that barring a few tests performed at lower temperature range in this work, the minimum specimen thickness requirement was not met in the present investigation and hence the J values reported in the present work are component specific and not material property.

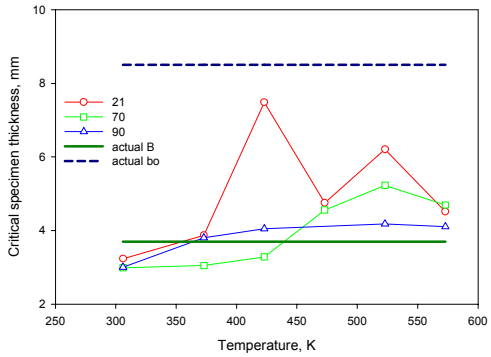

Fig. 7 Comparison of critical specimen dimension computed for samples containing different hydrogen content for a valid J_{IC} measurement with actual specimen dimension used in this work.

Formation of the CA-mesocracks in the mid-section of the specimens (fig.3) during fracture in Zr-2.5Nb pressure tube alloy has been reported by earlier investigators[9] also and have been attributed to the presence of sheafs of impurities such as chlorine, phosphorus, carbon, their complexes and precipitates like carbide and phosphides[4,8-9], which require lower energy to fracture. In the present investigation also qualitative composition analysis of the fracture surface using EDX probe indicated peaks corresponding to oxygen, carbon, silicon, chlorine and phosphorous. It may however be noted that since the fracture samples were cleaned ultrasonically in acetone for five minutes, the peaks

corresponding to the aforementioned elements were not very prominent for quantitative analysis. Thus in view of the forgoing it is felt that the CA-mesocracks seen in Fig. 3(a) for this alloy containing 21 ppm of hydrogen could be primarily due to the distribution and orientation of the trace impurities like Cl, P and carbon, its complexes and second phase particles. The role of circumferential hydrides is to link up these mesocracks as is evident from the longer cracks shown in fig. 3(b) for the sample containing 70 ppm of hydrogen.

It may be recalled that the formation of CA-mesocracks were more pronounced in the mid-section of the sample thickness as compared to the edges. Since the stress state in the mid-section of the sample is plane strain, the stress acting along the thickness of sample (along the radial direction of tube) could have resulted in the formation of these CA-mesocracks in the mid-section. On the other hand, the stress state near the sample surface is plane stress and hence the stress along sample thickness may not be sufficient to fracture these low energy areas, which explains why these CA-mesocracks were not observed near the sample surface[9].

One of the consequences of the formation of these mesocracks oriented along the circumferential-axial plane of the tube is the splitting of the sample thickness, thereby the thickness of the sample can be thought to be consisting of series of thinner samples[9]. Such a splitting of the sample thickness has been reported earlier also[9] and as a result the stress state ahead of the crack tip after the formation of these mesocracks will be closer to plane stress rather than plane strain resulting in increased toughness of the material. Since the hydride platelets facilitate the formation of larger CA-mesocraks, increase in hydride content could result in increase in toughness, thereby partially annulling the embrittlement effect of hydrides in these alloy. This probably could be the reason why the embrittlement effect of hydrides were not prominent for this alloy (Fig. 5).

Another interesting feature is the mild decrease observed in the fracture initiation parameters with increase in test temperature. Since with increase in test temperature vacancy concentration increase with increase in temperature, it is suggested the void nucleation will be easier resulting in decrease in fracture initiation parameters with increase in test temperature. Also, with increase in temperature, damage healing process in the material is likely to be more effective due to enhanced atomic mobility, which probably is the reason for the increase in fracture propagation parameters with increase in test temperature (fig.6).

V. CONCLUSIONS

It was observed that for a given test temperature both the fracture toughness parameters representing crack initiation and crack propagation decreased mildly with increase in hydrogen content whereas *dJ/da* was practically unaffected by hydrogen content.

The fracture surface showed large number of CA-mesocracks normal to crack growth plane. The circumferential hydrides were observed to increase the length of the CA-mesocracks by interlinking them and thus have the potential to reduce the fracture toughness.

However, the formation of the CA-mesocracks results change of the stress state from plane strain to plane stress and hence can enhance the fracture toughness. Due to the combined effect of two processes fracture toughness parameters are not significantly affected with increase in hydrogen content.

Also, for a given hydrogen content crack initiation fracture toughness parameters showed large scatter with a tendency to decrease with increase in test temperature whereas the crack propagation fracture toughness parameters increased with temperature to a saturation value.

ACKNOWLEDGEMENTS

Dr. Singh is on extraordinary leave from Bhabha Atomic Research Centre (BARC), Mumbai, India and is currently working as a Marie Curie Incoming International fellow at Malmo Högskola, which is financially supported by European Commission under its FP6 programme to promote researchers mobility into European Union. Constant encouragement and invaluable support provided by Dr. S. Banerjee, and Shri R. K. Sinha of BARC, Mumbai is acknowledged.

NOMENCLATURE

a_o	initial crack length after fatigue precracking
a	crack length (m) for edge crack and half crack length for body crack
A_{pl}	Area under the P vs. plastic LLD curve
b & b_o	Uncracked ligament
B	specimen or Tube thickness (m)
CCL	Critical crack length
CCT	Curved Compact Toughness
CWSR	Cold worked and stress relieved
D	Mean Diameter of tube
DCPD	Direct Current Potential Drop
dJ/da	Slope of the best fit line passing through qualified J values
Δa	Change in crack length
E	Young's Modulus
EDX	Energy Dispersive X-ray
$J_{0.15}$	J value for crack extension of 0.15 mm
$J_{1.5}$	J value for crack extension of 1.5 mm
J_{Max}	J value corresponding to Maximum load

K_I	stress intensity factor
K_{JC}	stress intensity factor computed from J_Q
K_{JMax}	stress intensity factor computed from J_{JMax}
LLD	Load Line Displacement
M	Folia's factor = $M = \sqrt{1+\frac{a^2}{rB}}$
MPa	Mega Pascal
MWe	Megawatt electrical
μm	micrometer
Nb	Niobium
ν	Poisson's ratio
O	Oxygen
P	Operating pressure
PHWR	Pressurized Heavy Water Reactor
ppm	Parts per million
P_Q	applied load (N)
r	Radius of tube
S_H	Hoop stress
σ_{flow}	Flow stress
σ_{UTS}	Ultimate Tensile strength
σ_{YS}	Yield strength
T	Temperature in K
UTM	Universal Testing Machine
W	specimen width (m)
Zr	Zirconium

REFERENCES

1. S. Glasstone and A. Sesonske, *Nuclear Reactor Engineering*, p-740, CBS publishers and Distributors, Delhi (India), 3rd edition., (1988).
2. W. Dietz, "Structural materials", *Materials Science & Techno. A Comprehensive treatment*, eds. R. W. Cahn, P. Haasen & E. J. Kramer, 10B Nuclear Materials, Chapter 8, 53 (1994).
3. C. Lemaignan and A. T. Motta, "Zirconium alloys in nuclear applications", *ibid* 10B chapter 7, 1 (1994).
4. C. E. Coleman, B. A. Cheadle, C. D. Cann and J. R. Theaker, "Development of pressure tubes with service life greater than 30 years", *Zr in the Nucl Ind.: 11th Intl. Symp., ASTM STP* **1295**, Eds. E. R. Bradley and G. P. Sabol, 884 (1996).
5. G. J. Field, J. T. Dunn, and B. A. Cheadle, *Can. Metall. Q.* **24**(3) 181 (1985).
6. M. P. Puls, *Nuclear Engg. & Design*, **171** 137 (1997).
7. G. D. Maon and P. J. Richinson, "Leak before break in CANDU pressure tubes: Recent advances", *Pressure vessel and piping conference 1993*, Denver, CO, USA, 25-29 Jul 1993, p-205 (1993).
8. J. R. Theaker, R. Choubey, G. D. Moan, S. A. Aldridge, L. Davis, R. A. Graham and C. E. Coleman, Fabrication of Zr-2.5Nb pressure tubes to minimize the harmful effects of trace elements, *Zr in the Nucl Ind.: 11th Intl. Symp.,, ASTM STP* **1295**, Eds. E. R. Bradley and G. P. Sabol 221 (1996).
9. P. H. Davies, R. R. Hosbons, M. Griffiths and C. K. Chow, "Correlation between Irradiated and Unirradiated fracture Toughness of Zr-2.5Nb pressure tubes", *Zr in Nucl Ind.: 10th Intl. Symp., ASTM STP* **1245**, Eds A. M. garde and E. R. Bradley, Philadelphia, p-135 (1994)
10. M. B. Elmoselhi, and B. D. Warr, A study of hydrogen uptake mechanism in zirconium alloys, *ibid.* p-62 (1994).
11. D. O. Northwood, and U. Kosasih, *Intl. Metals Rev.*, 28(2) 92 (1983).
12. R. N. Singh, S. Mukherjee, Anuja Gupta and S. Banerjee, *Jl. of Alloys and Comp.,* **389***, 102,* (2005).
13. Z. L. Pan, I. G. Ritchie and M. P. Puls, *Jl. of Nucl. Mater.*, **228**(2) 227 (1996).
14. P. H. Davies and C. P. Sterns, "Fracture toughness testing of zircaloy pressure tube material with radial hydrides using direct-current potential drop", *ASTM STP* ***905***, pp-379-400 (1986).
15. F. H. Huang, "Fracture toughness evaluation for zircaloy-2 pressure tubes with the electric-potential method", *ASTM Intl. Symp. On Small specimen test techniques applied to nuclear reactor vessel thermal annealing and plant life extension*, New Orlearns, LA, USA, 29-31 Jan 1992, pp-182-198 (1993).
16. K. S. Chan, *Acta Metall. Mater.* **43**(12) 4325 (1995).
17. L. A. Simpson and C. K. Chow, "Effect of metallurgical variable and temperature on the fracture toughness of zirconium alloys pressure tubes", *ASTM STP* **939** 579 (1987).
18. S. I. Honda, *Nucl. Engg. and Design*, **81** 509 (1984).
19. L. A. Simpson and C. D. Cann, *Jl. Nucl. Mater.*, **87** 303 (1979).
20. W. H. Erickson and D. Hardie, *Jl. Inst. of Metals*, **241** 444 (1964).
21. L. A. Simpson, *Metall.. Trans.***12A**, 2113 (1981).
22. R. N. Singh, R. Kishore, S. S. Singh, T. K. Sinha and B. P. Kashyap, *Jl. Nucl. Mater.* **325** 26 (2004).
23. A. C. Wallace, G. K. Shek and O. E. Lepik, "Effects of hydride morphology on Zr-2.5Nb fracture toughness", *Zr in Nucl. Ind.*: 8th Intl. Symp., Eds. L. F. P. Van Swam and C. M. Eucken, *ASTM STP* **1023**, 66 (1989).
24. R. N. Singh, Niraj Kumar, R. Kishore, S. Roychowdhury, T. K. Sinha and B. P. Kashyap, *Jl. Nucl. Mater.* **304**, 189 (2002).
25. M. P. Puls, *Metall. Trans. A* **21**A 2905 (1990).
26. D. Srivastava, G. K. Dey and S. Banerjee, *Metall. Trans. A,* **26A** 2707 (1995).
27. D. G. Westlake, *Jl. of Nucl. Mater.* **26**, 208 (1968).